Effect of silver content on the structure and antibacterial activity of silver-doped phosphate-based glasses

Sabeel P Valappil[1&2], David M Pickup[3], Donna L Carroll[4], Chris K Hope[5], Jonathan Pratten[2], Robert J Newport[3], Mark E Smith[4], Michael Wilson[2] and Jonathan C Knowles[1*].

[1]Division of Biomaterials and Tissue Engineering and [2]Division of Microbial Diseases , University College London, Eastman Dental Institute, 256 Gray's Inn Road, London. WC1X 8LD. UK. [3]School of Physical Sciences, University of Kent, Canterbury, CT2 7NH, UK. [4]Department of Physics, University of Warwick. Coventry, CV4 7AL, UK. [5]School of Dental Sciences, University of Liverpool, Edwards Building, Liverpool, L69 3GN. UK.

Running title: Antibiofilm activity of silver.

Key words: phosphate-based glasses; silver content; constant depth film fermentor; *Staphylococcus aureus; biofilms*

*****Corresponding Author. Mailing address: Division of Biomaterials and Tissue Engineering, UCL Eastman Dental Institute, 256 Gray's Inn Road, London WC1X 8LD. UK. Phone: +44 (0)207 915 1189, Fax: +44 (0)207 915 1227, Email:j.knowles@eastman.ucl.ac.uk

ABSTRACT

Staphylococcus aureus can cause a range of diseases such as osteomyelitis as well as colonize implanted medical devices. In most instances the organism forms biofilms that are not only resistant to the body's defence mechanisms but also display decreased susceptibility to antibiotics. In the present study, we have examined the effect of increasing silver content in phosphate-based glasses to prevent the formation of *S. aureus* biofilms. Silver was found to be an effective bactericidal agent against *S. aureus* biofilms and the rate of silver ion release (0.42-1.22 $\mu g.mm^{-2}. h^{-1}$) from phosphate-based glass was found to account for the variation in its bactericidal effect. Analysis of biofilms by confocal microscopy indicated that they consisted of an upper layer of viable bacteria together with a layer (~20μm) of non-viable cells on the glass surface. Our results showed that regardless of the silver contents in these glasses (10, 15 or 20 mol%) the silver exists in its +1 oxidation state which is known to be a highly effective bactericidal agent compared to other oxidation states (+2 or +3). Analysis of the glasses by ^{31}P NMR and HEXRD showed that it is the structural rearrangement of the phosphate network that is responsible for the variation in silver ion release and associated bactericidal effectiveness. Thus an understanding of the glass structure is important in interpreting the *in vitro* data and also has important clinical implications for the potential use of the phosphate-based glasses in orthopaedic applications to deliver silver ions to combat *S. aureus* biofilm infections.

INTRODUCTION

Staphylococcus aureus, a leading cause of nosocomial infections worldwide, is the aetiological agent of a wide range of diseases, from relatively benign skin infections to potentially fatal systemic disorders (41). Many of these diseases, including endocarditis, osteomyelitis, and foreign-body related infections, appear to be caused by biofilm-associated *S. aureus* (14, 18, 27, 38). Biofilms are sessile communities characterized by cells that are attached to a substratum or interface or to each other, embedded in a matrix of extracellular polymeric substances that they have produced, and exhibit an altered phenotype with respect to growth rate and gene transcription (14). Biofilm formation occurs as a result of a sequence of events: microbial surface attachment, cell proliferation, matrix production and detachment (34). Biofilm-associated bacteria show a decreased susceptibility to antibiotics (10), disinfectants (31) and clearance by host defences (14, 37). Work by Mulligan et al. (29, 30) showed that the inclusion of copper or silver ions in phosphate-based glasses was useful in treating biofilms of *Streptococcus sanguis.* Silver cations exhibit broad antimicrobial action at low concentrations, and they are already being used for the treatment of burn wounds (32) and traumatic injuries (5, 15). Feng et al. (15) studied the antibacterial effect of silver ions on *E. coli* and *S. aureus* and suggested that the antibacterial mechanism was due to DNA not being able to replicate, and proteins becoming inactivated after contact with silver ions.

Phosphate-based glasses are soluble materials that can act as a unique system for the delivery of silver ions in a controlled way (25). The ions are incorporated into the glass structure and are not a separate phase; thus, their rate of release is defined by the overall degradation rate of the glass. Phosphate-based glasses have already been used to deliver

70 silver ions to help control urinary tract infections in patients needing long-term
71 indwelling catheters (9, 17, 40) and also in wound dressings to prevent infections (9).
72 However in recent work, anomalies have been reported whereby the antimicrobial effect
73 does not follow an expected relationship with silver content (2). This is thought to be due
74 to the speciation and local coordination environment around the silver in the glass and,
75 more generally, the changes in the glass structure. Therefore the aims of this study were;
76 (a) to produce a range of silver-doped phosphate-based glasses (0, 10, 15 and 20 mol%
77 silver), (b) to measure the local coordination environment around the silver and (c) to
78 probe the glass structure and relate this to the results from *S. aureus* biofilm growth
79 studies. The findings from this study may lead to the potential use of the phosphate-based
80 glasses to deliver silver ions to combat *S. aureus* biofilm infections.
81
82 **MATERIALS AND METHODS**
83 **Bacterial strain and growth**
84 *Staphylococcus aureus* NCTC 6571 was routinely propagated on nutrient agar (Oxoid,
85 Basingstoke, UK) at 37°C. Nutrient broth (Oxoid) was used as the medium for the
86 constant depth film fermentor (CDFF) studies.
87 **Preparation of silver-doped phosphate-based glasses**
88 Phosphate-based glasses were produced using NaH_2PO_4 (BDH), P_2O_5 (Sigma), and
89 $CaCO_3$ (BDH). For the production of silver-containing phosphate-based glasses, Ag_2SO_4
90 (BDH) was also used as shown in Table 1. The amount of chemicals required for
91 particular composition were weighed and placed into a Pt/10%Rh crucible (Johnson
92 Matthey, Royston, UK) when non-silver-containing glasses were produced, while a

vitreous silica crucible (Saint-Gobain Quartz, Tyne & Wear, UK) was used when silver-containing glasses were produced (this was done to avoid silver forming alloys with platinum). The crucible was then placed in a preheated furnace at 1100°C for 1 hour. The molten glass was then poured into graphite moulds, which had been preheated to 370°C. The glass samples were allowed to cool to room temperature, and the resulting glass rods were cut into discs (5 mm diameter and 2 mm thickness) by using a rotary diamond saw (Testbourne Ltd., Basingstoke, UK).

Biofilm production

A CDFF (University College Cardiff, Cardiff, UK), described previously by Mulligan et al. (30), was used for the production of biofilms. The CDFF which contains a stainless steel turntable can hold up to 15 polytetrafluoroethylene (PTFE) pans; each PTFE pan can hold 5 PTFE plugs. Discs, 5 mm in diameter, were placed on each plug and recessed to a depth of 300 μm. The PTFE pans were then inserted so that they were flush with the turntable. A cylindrical glass vessel and two stainless steel end plates encase the turntable. The top plate contains an air inlet port, to which two 0.2 μm Hepa-vent air filters (Fisher Scientific, Town and Country) were attached. It also contains three media inlet ports. Incoming medium (in this case nutrient broth) drips onto the rotating turntable and is distributed over the PTFE pans by two scraper blades. The scraper blades also serve to maintain the biofilms on the discs at the required depth, equal to the depth of the recess. The bottom plate contains a medium outlet port. The CDFF was sterilized in a hot air oven, using a temperature of 160°C for 1 h. During all experiments, the CDFF was incubated at 37°C. The turntable rotated at a speed of 3 rpm.

Viable counts

At various time intervals, pans were removed aseptically from the CDFF. Each pan was washed with 10 ml of phosphate-buffered saline (PBS; Oxoid). Discs containing biofilms were placed in 1 ml of PBS and vortexed for 1 min to remove the attached biofilms and to disperse them into the suspension. Serial dilutions of the suspensions were carried out in PBS. 25 µl volumes of the suspension and each dilution were spread onto nutrient agar (Oxoid) plates. The plates were then incubated aerobically at 37°C for 48 h. For each type of disc, viable counts (colony forming units; CFUs) were conducted in triplicate.

Scanning electron microscopy (SEM)

Aseptically removed discs were placed in 3% glutaraldehyde in 0.1M sodium cacodylate buffer, to fix the cells, and stored at 4°C overnight. Specimens were then prepared for the scanning electron microscope by first dehydrating in a graded series of alcohols (20%, 50%, 70%, and 90%). The specimens were left in each alcohol for 15 min, before being rinsed three times in 100% alcohol (10 mins each time). Each specimen was then transferred into hexadimethylsilane for 2 mins prior to placing them in a desiccator. Once dry, the specimens were mounted onto aluminium stubs using araldite and sputter-coated with gold/palladium in a Polaron E5000 sputter coater. The specimens were then viewed with a Cambridge 90B SEM operating at 15 kV.

Confocal laser scanning microscopy (CLSM)

A viewing solution was first prepared containing 8ml of PBS together with 2 µl each of components A and B of BacLight™ LIVE/DEAD stain (Invitrogen, UK). The biofilm containing discs were placed into a small cell-culture dish (Bibby Sterilin Ltd, Stone,UK), and covered with the viewing solution and the stains were allowed to develop

139 in the dark for 10min. The biofilms were then examined via the microscope (Olympus
140 BX51 microscope) which incorporated a Bio-Rad Radiance 2100 laser scanning system
141 and LUMPlanFI 40x water lens. Two-channel (viable 'Live'/nonviable 'Dead') confocal
142 image stacks were collected in 8-bit colour depth at a resolution of 1024×1024 pixels.
143 The z-axis step size was typically 0.6 μm, however this was optimised for each image
144 stack depending upon the total depth of the sample.

145 **Image analysis**

146 The initial image analysis and 3D structure construction were performed using the Bio-
147 Rad LaserVox™ image analysis software whilst the structure and distribution of cell
148 vitality (19, 22) was elucidated using ImageJ (v1.33 u, National Institutes of Health,
149 USA). Projection images (plan view) were constructed to return the sum of pixel
150 brightness values through the entire image stack, effectively merging all the individual
151 sections into one greyscale image. The depth-related trends of the viable and nonviable
152 stains through the biofilms were determined by constructing fluorescence profiles. These
153 profiles were created by plotting the total image brightness, for each channel, against
154 depth into the image stack. These data were then normalised against the maximum
155 brightness value within their channel and converted into depth related viability profiles
156 by plotting the normalized viable fluorescence minus the normalised nonviable
157 fluorescence values against depth into the biofilms (19, 20).

158 **Statistical analysis**

159 One-way analysis of variance (ANOVA) was used to compare mean viable counts,
160 following arcsinh transformation of data. When a significant difference was detected, a

Tukey test was conducted to find which values were different (GraphPad Software; San Diego, USA.).

Glass degradation and ion release

Degradation study

Silver-doped phosphate-based glass rods (5 mm diameter and 2 mm thickness) with different contents of silver ions were placed in plastic containers and filled with 50 ml of deionised water (pH 7±0.5), and placed in an incubator at 37°C. At various time points (6, 24, 48, 120 and 144h) the three disks were taken out of their respective containers, and excess moisture was removed by blotting the samples dry with tissue prior to weighing them. All the disks were placed into a fresh solution of deionised water and placed back into the 37°C incubator. To obtain the rate of weight loss, the initial weight (M_0) of each sample was measured as well as the weight at time t (M_t) to give a weight loss per unit area thus: weight loss=$(M_0–M_t)/A$, where A is the surface area (mm^2). The measurements were carried out in triplicate. The data were plotted as weight loss per unit area against time. The slope of this graph gave a dissolution rate value in terms of $mg.mm^{-2}\ h^{-1}$, which was determined by fitting a straight line of the form $y = mx$ through the origin.

Ion release study

Ion release studies were simultaneously conducted, and the medium was analysed for cation (Na^+ and Ca^{2+}) and anion (PO_4^{3-}, $P_2O_7^{4-}$, $P_3O_9^{3-}$ and $P_3O_{10}^{5-}$) release using ion chromatography (Dionex, UK). Silver ion release was measured using the commercially available silver test kit (Silver Test Kit 1.14831.0001, Merck, UK). The test works on the

principle that in a weakly acidic solution, silver ions react with phenanthroline and eosine to form a red complex, the concentration of which is determined photometrically (at 552 nm). A silver standard solution, 1000 mg/l Ag, provided by the supplier, was used to prepare the calibration curve. In the event of silver concentrations exceeding 5 mg/l, samples were diluted before measurement. For all samples tested, high purity water was used as a reference.

Structural analysis of the silver-doped phosphate-based glasses

^{31}P MAS NMR

All ^{31}P NMR experiments were performed using a Varian-Chemagnetics CMX 360 MHz Infinity spectrometer equipped with an 8.45 T magnet operating at a frequency of 145.85 MHz. A Varian 4 mm probe was used and the samples were spun at ~12 kHz. A standard one pulse experimental procedure was used. A single pulse of 1.4 μs (corresponding to a tip angle of 30°) and a recycle delay of 450 s were used due to the extremely long T_1 relaxation time of ~360 s. The spectra were referenced against a secondary reference of $NH_4H_2PO_4$ at a shift of +0.9 ppm (relative to 85 % H_3PO_4).

High energy X-ray diffraction

The high energy X-ray diffraction (HEXRD) data were collected on Station 9.1 at the Synchrotron Radiaton Source (SRS) Daresbury Laboratory, UK. The finely powdered samples were enclosed inside a 0.5 mm thick circular metal annulus by kapton windows and mounted onto a flat-plate instrumental set-up. The wavelength was set at $\lambda = 0.5092$ Å, and calibrated using the K-edge of a Pd foil; this value was low enough to provide

data to a high value of momentum transfer ($Q_{max} = 4\pi\sin\theta/\lambda \sim 22$ Å^{-1}). The data were corrected using a collection of programs written in-house.

The initial stage of analysis of X-ray diffraction data from an amorphous material involves the removal of background scattering, normalization, correction for absorption and subtraction of the self-scattering term (13). The resultant scattered intensity, *i(Q)*, can reveal structural information by Fourier transformation to obtain the pair distribution function:

$$T(r) = T^0(r) + \int_0^\infty Qi(Q)\sin(Qr)\,d(Q)$$

where $T^o(r) = 2\pi^2 r\rho_o$ (r is the atomic separation between atoms and ρ_o is the macroscopic number density)

Ag K-edge XANES measurements

Ag K-edge X-ray absorption spectroscopy (XAS) measurements were made at a temperature of approximately 77 K on Station 16.5 at the SRS. The spectra were recorded in transmission mode using a double crystal Si(220) monochromator and ionisation chambers to detect the incident and transmitted beam intensities, I_i and I_t respectively. A silver foil and a third ionisation chamber were placed after the sample's transmission ionisation chamber to allow an absorption spectrum of the foil to be collected simultaneously for the purpose of calibration of the energy scale. The energy scale was defined by assigning the maximum of the derivative of the Ag foil spectrum to 25521.0 eV.

The data processing comprised conversion of the data to absorption *versus* energy, calibration of the energy scale, removal of the pre-edge absorption by straight-line fitting to $Log_{10}(I_i/I_0)$ and removal of the post-edge atomic absorption profile by fitting with a

second order polynomial. All the spectra were normalised to have an edge-step of unity. Spectra were also collected from reference materials; AgO (Aldrich), and Ag_2SO_4 (≥99.99%, Aldrich).

RESULTS

SEM analysis of the attachment of *S. aureus* to silver-doped phosphate-based glasses

SEM analysis of *S. aureus* biofilms on hydroxyapatite (HA), Ag-, Ag10, Ag15 and Ag20 discs showed reduction in *S. aureus* attachment on Ag10, Ag15 and Ag20, with Ag20 being the least, compared to Ag- and HA discs (data not shown).

Effect of increasing silver ion concentration on the viable counts of *S. aureus* in biofilms for 48 h

Initial viable count experiments were conducted on Ag10, Ag15 and Ag20 (Table 1). Both Ag- and HA discs were used as controls (Figure 1). Each point represents the $\log_{10}$ of the mean number of viable count of three biofilms from one representative CDFF run. Error bars represent standard deviations. It should be noted that at least three runs for each experiment were performed to confirm the results found. The data were not pooled because slight differences in the inoculation produced differences in the absolute CFU numbers obtained. However, the relative differences found were very repeatable.

(a) Ag10

The Ag10 glasses showed no significant difference between the $\log_{10}$ of the mean number of viable cells (6.08±0.11) compared to both Ag- (6.11±0.13) (p=0.77) and HA discs (6.19±0.12) (p =0.11) at 6h (Figure 1). However, at 24h, the Ag10 discs displayed statistically significant ($p \leq 0.001$) difference between the $\log_{10}$ of the mean number of

252 viable cells (4.65±0.17) compared to both the controls, Ag- (6.32±0.32) and HA discs
253 (6.37±0.11). The $\log_{10}$ of the mean number of viable cells at 48h on Ag10 discs
254 (6.42±0.08) started to recover from the previous low at 24h, but was still less than both
255 the controls, Ag- (8.21±0.06) (p =0.0001) and HA (7.96±0.33) (p =0.001). There was
256 approximately a 1.2 $\log_{10}$ reduction in CFUs for the Ag10 glasses compared to controls
257 that were maintained for the first 48 h.

258 **(b) Ag15**

259 Similar to the Ag10 glasses, the Ag15 glasses also showed no significant difference
260 between the $\log_{10}$ of the mean number of viable cells (6.02±0.20) compared to both the
261 Ag- discs (6.12±0.13) (p=0.51) and HA discs (6.19±0.13) (p =0.28) at 6h (Figure 1). By
262 24 h, the Ag15 discs (4.03±0.11) displayed a statistically significant (p ≤0.0003)
263 difference in the $\log_{10}$ of the mean number of viable cells compared to both the controls,
264 Ag- (6.33±0.32) and HA discs (6.37±0.11). Similar to the Ag10 glasses, the $\log_{10}$ of the
265 mean number of viable cells at 48h on Ag 15 discs (7.14±0.13) started to recover from
266 the previous low at 24h but was still less than both the controls, Ag- (8.21±0.06) (p
267 =0.0002) and HA discs (7.96±0.33) (p =0.002). There was an approximately 1.5 $\log_{10}$
268 reduction in CFUs maintained for the first 48 h by Ag15 glasses compared to the
269 controls.

270 **(c) Ag20**

271 Only the Ag20 glasses showed a statistically significant difference in the $\log_{10}$ of the
272 mean number of viable cells (5.44±0.24) compared to both the Ag- (6.11±0.13)
273 (p=0.015) and HA discs (6.19±0.13)(p =0.01) at 6 h (Figure 1). As with the other glasses,
274 the $\log_{10}$ of the mean number of viable cells at 24h on the Ag20 discs (5.10±0.04) started

to recover from the previous low at 6h, but showed a statistically significant difference to both the controls, Ag- (6.33±0.32) (p =0.003) and HA discs (6.37±0.11) (p =0.0001). After 48 h, the Ag20 discs (7.26±0.21), displayed a significant difference in CFUs compared to the controls, the Ag- (8.21±0.06) (p =0.002) and HA discs (7.96±0.33) (p =0.036). There was an approximately 1 $\log_{10}$ reduction in CFUs that was maintained for the first 48 h by the Ag20 glasses compared to the controls.

Due to the early onset of a bactericidal effect (from 6h of biofilm growth) by the Ag20 glasses, it was chosen along with Ag15 glasses (which displayed maximum bactericidal effect at 24 h of biofilm growth compared to other glasses) for the second set of CDFF studies with time points up to 144h.

Effect of Ag15 glasses on viable counts of *S. aureus* biofilms up to 144h

In the second set of experiments, the Ag15 glasses showed no significant difference in the $\log_{10}$ of the mean number of viable cells (5.79±0.08) compared to the Ag- discs (5.97±0.11) (p=0.084), but a statistically significant difference from HA discs (6.36±0.19) (p =0.009) at 6h (Figure 2). The difference in CFUs became more apparent at 24h as the Ag15 (4.56±0.2) displayed a statistically significant ($p \leq 0.002$) difference in the $\log_{10}$ of the mean number of viable cells compared to both the controls, the Ag- (7.29±0.09) and HA discs (7.02±0. 0.57). After 48 h, the $\log_{10}$ of the mean number of viable cells on the Ag15 (6.80±0.49) started to recover from the previous low at 24h, but was still less than both the controls, the Ag- (7.85±0.15) (p =0.024) and HA discs (7.9±0.15) (p =0.021). However, at time points > 48 h, the Ag15 glasses showed a sharp increase in the CFUs compared to the controls and the $\log_{10}$ CFU for all samples reached

297 values similar to those for the controls by 120h and remained similar, at approximately
298 8.3 $\log_{10}$ CFU, until 144 h (Figure 2).

299 **Effect of Ag20 glasses on viable counts of *S. aureus* biofilms up to 144h**

300 The Ag20 glasses showed the greatest difference in the $\log_{10}$ of the mean number of
301 viable cells (5.33±0.20) compared to both the Ag- (6.31±0.11) (p=0.002) and HA discs
302 (6.23±0.16)(p =0.004) at 6h (Figure 3). As in the first set of CDFF runs, the $\log_{10}$ of the
303 mean number of viable cells at 24 on the Ag20 (5.66±0.07) discs started to recover from
304 the previous low at 6 h, but showed a significant difference to both the controls, the Ag-
305 (7.±0.18) (p =0.0003) and HA discs (7.23±0.03) (p =0.0001). This effect continued at 48h
306 with the Ag20 discs (7.57±0.16), displaying a significant difference to both the controls,
307 the Ag- (8.27±0.03) (p =0.002) and HA discs (8.42±0.05) (p =0.0009). Compared to the
308 Ag15 glasses, at 120h, the $\log_{10}$ CFUs on the Ag20 glasses stayed at a reduced level
309 (8.05±0.24) compared to the Ag- discs (8.51±0.19) (p=0.03), but did not exhibit any
310 statistically significant difference from HA discs (8.59±0.40) (p =0.096). More
311 importantly, at longer time points, the $\log_{10}$ CFUs stayed at a reduced level,
312 approximately 0.6 $\log_{10}$ CFU reductions, compared to both the controls ($p \leq 0.005$) even
313 until 144 h (Figure 3).

314 **Identification of dead bacterial layers using CLSM**

315 The use of water immersion lenses and a liquid viewing medium (PBS) in the present
316 study enabled the observation of biofilms in their natural hydrated state (Figure 4).
317 Viability mapping, as described by Hope et al. (20), which encompasses viability changes
318 in the z axis was performed (Figure 5). As seen in normal viewing of BacLight™
319 LIVE/DEAD stained images, in the present study, the viable cells fluoresce green and the

nonviable cells fluoresce red (Figure 4). The biofilms were submerged in the stains (at a relatively high concentration) for at least 15 min before the CLSM scan. The molecular weights of the BacLight^{TM} LIVE/DEAD stain components are similar (component A= 550–750 Da (proprietary information) and component B = 668.4 Da), and both have a net positive charge. It is therefore unlikely that there is any significant difference in their diffusion characteristics into biofilms. The viability distributions in the biofilms were observed in this study using CLSM image analysis. Regions of biofilms composed of viable bacteria with a layer of non-viable bacteria at the interface with the antimicrobial-releasing materials were analysed further (Figure 5).

Viability mapping

Depth-related viability profiles (Figure 5) through the 2 day-old biofilms returned positive values (i.e. increasing) in the upper ~20 μm of the confocal image stack. This indicated that the proportion of viable fluorescence, compared to nonviable fluorescence, increased with depth (i.e. the vertical distance into the biofilm from its highest point) in this region. Between a depth of ~20 and ~40μm, the viability profile values decreased, suggesting that the proportion of viable fluorescence decreased. Moreover, at these depths the viability profiles values fluctuated from low to high. This may be because the confocal laser/fluorophore emissions becoming absorbed by the biofilm, causing a corresponding reduction in the brightness of the optical sections.

Degradation and ion release of silver-doped phosphate-based glasses

The degradation rates obtained, by applying a line of best fit through the weight loss per unit area of each glasses against time (data not shown), for the Ag10, Ag15 and Ag20

343 glasses were 1.22, 0.41 and 0.42 $\mu g.mm^{-2}.h^{-1}$ respectively (Figure 6). Both the Ag15 and
344 Ag20 glasses showed no perceptible differences in their degradation rate profiles (Figure
345 6). However, the profile of the Ag10 glasses did exhibit an increased degradation rate
346 compared to Ag15 and Ag20 glasses. The result showed that rate of silver ion release is
347 correlated to rate of degradation with statistically significant ($p \leq 0.005$) difference
348 between Ag10 compared to Ag15 and Ag20 but no significant difference ($p \geq 0.692$)
349 between Ag15 and Ag20 glasses (Figure 6). Rate of release of other cations such as Na^{+}
350 displayed statistically significant ($p \leq 0.016$) difference between Ag10 compared to Ag15
351 and Ag20 but no statistical difference ($p \geq 0.666$) between Ag15 and Ag20 glasses (Figure
352 6). Similarly, with Ca^{2+} ion, statistically significant ($p \leq 0.0001$) difference was observed
353 only between Ag10 compared to Ag15 and Ag20 but not between Ag15 and Ag20
354 glasses ($p \geq 0.167$). Among the anions (PO_4^{3-}, $P_2O_7^{4-}$, $P_3O_9^{3-}$ and $P_3O_{10}^{5-}$), $P_3O_9^{3-}$ was the
355 anion released to the greatest extent and it was also found to correlate strongly with rate
356 of degradation of the glasses (Figure 6). As in the case of cations, the rate of $P_3O_9^{3-}$ ion
357 release showed statistically significant ($p \leq 0.016$) difference between Ag10 compared to
358 Ag15 and Ag20 but no significant difference ($p \geq 0.666$) between Ag15 and Ag20 glasses.
359
360 Due to the importance of silver release in this study, the actual amount of silver ion
361 released at each time point is highlighted in figure 7. As expected, no silver was detected
362 from the Ag- glasses throughout the silver release study. At 6h, there were no significant
363 difference ($p \geq 0.066$) in silver ion release among Ag10, Ag15 and Ag20 glasses (Figure 7)
364 which continued up to 48h between Ag10 and Ag20 glasses($p \geq 0.078$). Ag20 released
365 higher amounts of silver at 24 and 48h compared to Ag15, but there were no significant

366 difference in the silver ion release at 120 and 144h between Ag15 and Ag20 glasses
367 ($p \geq 0.09$). However, from 48h onwards the Ag10 glasses released the highest amount of
368 silver ions compared to both Ag15 and Ag20 glasses (Figure 7).
369
370 **Structural analysis of the silver-doped phosphate-based glasses**
371 Examining the results in Figure 1 for the bactericidal effectiveness of the silver-doped
372 phosphate-based glasses on *S. aureus* biofilms after 48 h, excellent correlation with the
373 silver release curve shown in Figure 6 was found: above 10 mol% silver, there was a
374 reduction in both the bactericidal activity and silver ion release. The reduction in silver
375 ion release also correlated with a flattening out of the rate of degradation curve in Figure
376 6, where the expected (on the basis of the relative solubilities of sodium and silver salts)
377 reduction in dissolution rate with increasing substitution of silver ions for sodium ions did
378 not continue above 15 mol%. In order to understand the variation of properties with silver
379 content, the structure of the glass was examined using, ^{31}P MAS NMR, high-energy XRD
380 and Ag K-edge XANES.
381 The structure of phosphate glasses is know to consist of PO_4^{3-} tetrahedra connected
382 together by between 1 and 3 bridging oxygen atoms (BOs) to form a network (8). The
383 connectivity of this phosphate network is commonly described by Q^n notation, where n
384 refers to the number of BOs in the PO_4^{3-} group. Thus a Q^3 PO_4^{3-} unit has 3 BOs to other
385 PO_4^{3-} units and one non-bridging oxygen (NBO), whereas a Q^0 PO_4^{3-} unit has 4 NBOs
386 and is unconnected to other PO_4^{3-} groups. This connectivity is affected by the glass
387 composition. Vitreous P_2O_5 has a structure composed entirely of Q^3 units; whereas

388 addition of metal oxides to phosphate glasses reduces this connectivity and introduces Q^1
389 and Q^2 groups into the structure.

390 In the ^{31}P MAS NMR spectra for the silver-doped phosphate-based glasses, shown in
391 Figure 8, the single most prominent peak observed occurs at a chemical shift of -27 ppm
392 and is assigned to Q^2 groups (26). Two weaker resonances are also observed at -6 and -37
393 ppm; the latter manifests itself as a broad tail on the low chemical shift side of the main
394 peak. They are assigned to the presence of phosphorus in Q^1 and Q^3 environments,
395 respectively The presence of Q^1 and Q^3 environments in samples containing $\geq$ 10 mol%
396 silver is indicative of disproportionation of Q^2 units according to the equation,
397 $2Q^2 \rightarrow Q^1 + Q^3$. In other words, Q^2 groups, which are the structural units that make up
398 phosphate chains and rings, are converting to Q^1 units, which represent P_2O_7 dimers and
399 chain-terminating phosphate groups, and Q^3 groups, which represent cross-linking
400 between the phosphate chains. Examining Figure 8, it can be seen that the intensity of the
401 Q^1 and Q^3 features increases with silver content, suggesting a structural change in the
402 glass that occurs as a function of silver content. The ^{31}P NMR results therefore show that
403 as the silver content of these glasses increases, there is a structural change from
404 phosphate rings and polymeric chains to shorter, more cross-linked chains.

405 The HEXRD pair-distribution functions shown is Figure 9 give information on the
406 average P-O bonding in the glasses. The peak centred at ~1.55 Å in these functions is
407 composed of two components: a shorter distance of ~1.49 Å due to P-NBO bonds and a
408 longer distance of ~1.60 Å P-BO bonding (8). It can be seen from Figure 9 that the shape
409 of the P-O peak in the samples studied here changes as the silver content increases (10 →
410 20 mol%). This change reflects a change in the distribution of BOs and NBOs between

411 phosphorus atoms as a function of silver content, consistent with Q^2 groups
412 disproportionating into Q^1 and Q^3 groups. In agreement with the ^{31}P NMR data, this result
413 suggests a change in the connectivity of the phosphate network with higher silver
414 loadings.
415 The Ag K-edge XANES measurements yield information on the oxidation state of silver
416 and its local structural environment. The XANES spectra from the three silver-doped
417 phosphate glasses studied here were identical, demonstrating that the oxidation state and
418 local environment of silver is the same in each. For this reason only the spectrum from
419 the Ag10 glass is shown in Figure 10. The Ag K-edge XANES spectra from the reference
420 compounds are also shown in Figure 10. The position of the X-ray absorption edge in
421 each spectrum contains information on the oxidation state of the silver present. The edge
422 position of AgO, which contains a mixture of Ag^I and Ag^{III} ions (28), appears at the
423 highest energy since it requires more energy to remove electrons from the higher valence
424 ions. The absorption edges of Ag^I compounds appear at lower energy. The edge positions
425 of the silver-doped phosphate glasses all overlay the edge position of Ag_2SO_4. Given that
426 Ag_2SO_4 is a Ag^I compound, this result suggests that the silver in the glasses is present as
427 Ag^I. The similarity in the shape of the XANES spectra from the phosphate glasses and
428 that from Ag_2SO_4 suggests that the structural environment of silver in the glasses is
429 similar to that in the sulphate. Since Ag_2SO_4 contains silver ions surrounded by a
430 distorted octahedron of oxygen atoms (16), it follows that the silver ions in the
431 phosphate-based glasses reside in a very similar environment.
432
433

DISCUSSION

Previous work suggests that silver-doped phosphate-based glasses, with a fixed phosphate content of 50 mol % and a fixed calcium oxide content of 30 mol %, are capable of broad-spectrum bactericidal activity against planktonic bacteria including *S. aureus* (2). However, in a biofilm environment, microbes exhibit reduced susceptibility to antimicrobial agents. Silver has shown to be bactericidal against *Streptococcus sanguis* biofilms when phosphate-based glasses were used as a means of delivering the ions in a controlled manner (30). The results of the present study show that the release of an optimal amount of silver ions from the silver-doped phosphate-based glasses that can cause significant reduction of *S. aureus* biofilm growth occurs in 24h. From this point onwards the silver ions released from the glasses did not prevent the re-emergence of viable bacteria from the biofilms (Figure 1). Moreover the CLSM analysis confirmed the production of a dead bacterial layer at the interface between the biofilm and the silver-releasing phosphate-based glasses (Figure 5b).

Chaw et al. (11) reported that low concentrations of silver ions are unsuitable for the treatment of biofilm infections. Although higher silver concentrations have increased effectiveness against sessile cells (3, 30), they nevertheless face the challenge of maintaining their ionic form in applications containing large amount of halides and other ions (e.g. Cl^-, HCO_3^- and CO_3^-) and proteins (24, 35) due to the production of the insoluble silver salts, which results in silver ion inactivity. As silver ions are highly reactive and bind strongly to the electron donor groups containing oxygen or nitrogen (36) in the extracellular matrix (EM), we suggest that they must be able to bind to molecules such as proteins and polysaccharides within the EM. Therefore it is plausible

457 that the formation of a dead bacterial layer (Figure 5b) at the interface with the silver
458 releasing phosphate-based glasses resulted in re-emergence of viable bacteria after 24h
459 growth of *S .aureus* in the present study. Other factors, such as the diffusion limitation of
460 silver ions from the phosphate-based glasses or the switching on/off of quorum sensing
461 signals that triggered the efflux pump, which protected *S. aureus* from the toxic silver
462 ions need to be addressed.
463 Viability mapping can be used to examine the penetration of the bactericidal effect of
464 antimicrobial compounds into biofilms. Whilst it is obviously useful to make direct
465 measurements of the penetration of the antimicrobial compound itself (usually by
466 microelectrodes) into the biofilm, it is the penetration of the antimicrobial effect that is of
467 greater importance with regard to the remediation of the most recalcitrant microbial
468 biofilms (22). The fidelity of BacLight^{TM} LIVE/DEAD stain does not allow one to
469 categorically state that an individual cell which has taken up the nonviable stain
470 (propidium iodide) is unable to reproduce in culture (4). However it is sufficient to allow
471 us to visualize gradients in the spatial distribution of these stains and interpret these
472 motifs as indicators of gradients in cell vitality. In a recent study Beyenal et al. (7) used
473 an optical microsensor to probe biofilms of *S. aureus* which were labelled with a yellow
474 fluorescent protein. The microsensor measured fluorescence in the biofilms directly and
475 reported depth-related profiles similar to the bell-curves obtained by CLSM (21). This
476 suggested that metabolic activity (vitality) increases with depth in the outer layers of a
477 biofilm before decreasing in the deeper regions.
478 Although high concentrations of free silver ions are needed for bactericidal action against
479 biofilms, it is very important not to sacrifice any cyto/biocompatibility aspects of the

480 material while maintaining an effective antimicrobial effect. The amount of silver
481 released from silver-doped glasses investigated in this study is well below the levels that
482 are cytotoxic for human cells (33). The report suggested that the minimum bactericidal
483 concentration of silver is 0.1 ppm, and the cytotoxic concentration is 1.6 ppm for human
484 cells (33). The actual amounts quantified from the profiles observed in Figure 7, were
485 respectively 0.083, 0.055 and 0.064 ppm.h^{-1} for the Ag10, Ag15 and Ag20 glasses. All
486 within the limits specified above. However, it must be noted that it was unclear if the
487 levels of 0.1ppm and 1.6ppm stated by Saravanapavan et al. (33) were total values, or
488 whether they were rates in hours or days etc.
489 The structural analysis using ^{31}P NMR revealed that Q^2 species are the dominant
490 structural unit in the glasses investigated. This agrees with the predicted model for
491 metaphosphate glasses (i.e. 50 mol% P_2O_5) where the network should be based
492 exclusively on Q^2 tetrahedra, forming chains and/or rings (1, 8). Recently it was found
493 that the phosphate network was unaltered by exchanging sodium with silver for up to one
494 quarter of the initial sodium content (Ahmed et al. unpublished results). This also
495 correlated well with the XRD studies where the crystalline phase identified after
496 annealing the glass at glass crystallisation temperature, T_c, was a cyclic Q^2 species
497 (namely, P_3O_9).
498 As can be observed from the dissolution profiles in Figure 6, for silver-doping levels
499 above 10 mol%, the rate of release of silver ions decreases and the overall degradation of
500 the glass stabilises. This change can be correlated with a structural change that can be
501 observed in the ^{31}P NMR and HEXRD results. This change is related to a rearrangement
502 of the phosphate network from Q^2 chains and rings to shorter, more branched chains as

503 indicated by the presence of increasing amounts of Q^1 and Q^2 species with increasing
504 silver content. The Ag K-edge XANES spectra from the Ag10, Ag15 and Ag20 glasses
505 are all identical confirming that there is no change in the silver oxidation state or local
506 environment as a function of silver content. Given this, we can conclude that it is the
507 structural rearrangement of the phosphate network that is responsible for the variation in
508 silver ion release and associated bactericidal effectiveness. The literature shows that
509 silver in its +1 oxidation state is highly effective against planktonic bacteria (6, 15, 23).
510 The Ag K-edge XANES spectra from the glasses studied here confirm that the silver is
511 present as Ag^I in all three compositions.
512 Apart from the current applications, such as coating of a catheter with silver ions to avoid
513 bloodstream infections (12, 39), a strategy of using the silver ions' bactericidal effect on
514 biofilms in combination with other antimicrobial ions, such as copper zinc or gallium, can
515 be explored for the future testing of antimicrobial effectiveness. This synergistic approach
516 may work well with the silver ions destabilizing the biofilm matrix with other
517 antimicrobial ions and subsequently killing the bacteria.
518

519 **ACKNOWLEDGEMENTS**

520 We thank following people from UCL Eastman Dental Institute, UK, for their help on
521 various aspects of the work; Miss. Farah Dalwai (CDFF), Mr. Will Koning and Dr.
522 Ensanya Abou Neel (CLSM) and Mrs. Nicky Morden (SEM) . This work was supported
523 by the EPSRC, UK grant no. GR/T21080/01, EP/C000714/1 and EP/C000633/1. We also
524 thank B. Bilsborrow and M.A. Roberts of the CCLRC Daresbury Laboratory for their
525 assistance in the use of instruments 16.5 and 9.1 respectively.

REFERENCES

1. **Ahmed, I., M. P. Lewis, Olsen. I, and J. C. Knowles.** 2004. Phosphate glasses for tissue engineering: part 1. processing and characterisation of a ternary based P_2O_5-CaO-Na_2O glass system. Biomaterials **25:**491-499.

2. **Ahmed, I., D. Ready, M. Wilson, and J. C. Knowles.** 2006. Antimicrobial effect of silver-doped phosphate-based glasses. J. Biomed. Mater. Res. A. **79:**618-626.

3. **Akiyama, H., O. Yamasaki, H. Kanzaki, J. Tada, and J. Arata.** 1998. Effects of sucrose and silver on *Staphylococcus aureus* biofilms. J. Antimicrob. Chemother. **42:**629-634.

4. **Amor, K. B., P. Breeuwer, P. Verbaarschot, F. M. Rombouts, A. D. Akkermans, W. M. De Vos, and T. Abee.** 2002. Multiparametric flow cytometry and cell sorting for the assessment of viable, injured, and dead bifidobacterium cells during bile salt stress. Appl. Environ. Microbiol. **68:**5209-5216.

5. **Becker, R. O.** 1999. Silver ions in the treatment of local infections. Metal-Based Drugs **6:**311-314.

6. **Bellantone, M., H. D. Williams, and L. L. Hench.** 2002. Broad-spectrum bactericidal activity of Ag_2O-doped bioactive glass. Antimicrob. Agents. Chemother. **46:**1940-1945.

7. **Beyenal, H., C. Yakymyshyn, J. Hyungnak, C. C. Davis, and Z. Lewandowski.** 2004. An optical microsensor to measure fluorescent light intensity in biofilms. J. Microbiol. Method. **58:**367-374.

8. **Brow, R. K.** 2000. The structure of simple phosphate glasses. J. Non-Crystal. Solids. **263:**1-28.

9. **Cartmell, S. H., P. J. Doherty, N. P. Rhodes, J. A. Hunt, D. M. Healy, and T. Gilchrist.** 1998. Haemocompatiblity of controlled release glass. J. Mater. Sci. Mater. Med. **9:**1-7.

10. **Ceri, H. M., E. Olson, C. Stremick, R. R. Read, D. Morck, and A. Buret.** 1999. The calgary biofilm device: new technology for rapid determination of antibiotic susceptibilities of bacterial biofilms. J. Clin. Microbiol. **37:**1771-1776.

11. **Chaw, K. C., M. Manimaran, and F. E. H. Tay.** 2005. Role of silver ions in destabilization of intermolecular adhesion forces measured by atomic force microscopy in *Staphylococcus epidermidis* biofilms. Antimicrob. Agents. Chemother. **49:**4853-4859.

12. **Cicco, M. D., C. Campisi, and M. Matovic.** 2003. Central venous catheter-related bloodstream infections: pathogenesis factors, new perspectives in prevention and early diagnosis. J. Vasc. Access. **4:**83-91.

13. **Cole, J. M., E. R. H. van Eck, G. Mountjoy, R. Anderson, T. Brennan, G. Bushnell-Wye, R. J. Newport, and G. A. Saunders.** 2001. An x-ray diffraction and ^{31}P MAS NMR study of rare-earth phosphate glasses, $(R_2O_3)_x(P_2O_5)_{1-x}$, x = 0.175-0.263, R = La, Ce, Pr, Nd, Sm, Eu, Gd, Tb, Dy, Ho, Er. J. Phys: Condes. Matter. **13:**4105-4122.

14. **Donlan, R. M., and J. W. Costerton.** 2002. Biofilms: survival mechanisms of clinically relevant microorganisms. Clin. Microbiol. Rev. **15:**167-193.

15. **Feng, Q. L., J. Wu, G. Q. Chen, F. Z. Cui, T. N. Kim, and J. O. Kim.** 2000. A mechanistic study of the antibacterial effect of silver ions on *Escherichia coli* and *Staphylococcus aureus*. J. Biomed. Mater. Res. **52:**662-668.

16. **Fletcher, D. A., R. F. McMeeking, and D. Parkin.** 1996. The United Kingdom chemical database. J. Chem. Inf. Comput. Sci. **36:**746.

17. **Gilchrist, T., D. M. Healy, and C. Drake.** 1991. Controlled silver-releasing polymers and their potential for urinary-tract infection control. Biomaterials **12:**76-78.

18. **Gotz, F.** 2002. Staphylococcus and biofilms. Mol. Microbiol. **43:**1367-1378.

19. **Hope, C. K., D. Clements, and M. Wilson.** 2002. Determining the spatial distribution of viable and nonviable bacteria in hydrated microcosm dental plaques by viability profiling. J. Appl. Microbiol. **93:**448-455.

20. **Hope, C. K., and M. Wilson.** 2004. Analysis of the effects of chlorhexidine on oral biofilm vitality and structure based on viability profiling and an indicator of membrane integrity. Antimicrob. Agents. Chemother. **48:**1461-1468.

21. **Hope, C. K., and M. Wilson.** 2006. Biofilm structure and cell vitality in a laboratory model of subgingival plaque. J. Microbiol. Methods. **66:**390-398.

22. **Hope, C. K., and M. Wilson.** 2003. Measuring the thickness of an outer layer of viable bacteria in an oral biofilm by viability mapping. J. Microbiol. Methods. **54:**403-410.

23. **Kim, T. N., Q. L. Feng, J. O. Kim, J. Wu, H. Wang, G. C. Chen, and F. Z. Cui.** 1998. Antimicrobial effects of metal ions (Ag^{+}, Cu^{2+}, Zn^{2+}) in hydroxyapatite. J. Mater. Sci. Mater. Med. **9:**129-134.

24. **Klasen, H. J.** 2000. A historical review of the use of silver in the treatment of burns. II. renewed interest for silver. Burns **26:**131-138.

25. **Knowles, J. C.** 2003. Phosphate based glasses for biomedical applications. J. Mater. Chem.**13:**2395-2401.

26. **Mackenzie, K. J. D., and M. E. Smith.** 2002. Multinuclear solid state NMR of inorganic materials. Pergamon Press.UK.

27. **Mayberry-Carson, K. J., B. Tober-Meyer, J. K. Smith, J. Lambe, D.W., and J. W. Costerton.** 1984. Bacterial adherence and glycocalyx formation in osteomyelitis experimentally induced with *Staphylococcus aureus*. Infect. Immun. **43:**825-833.

28. **McKeown, D. A., H. Gan, and I. L. Pegg.** 2005. Silver valence and local environments in borosilicate and calcium aluminoborate waste glasses as determined from X-ray absorption spectroscopy. J. Non-Crystal. Solids.. **351:**3826-3833.

29. **Mulligan, A. M., M. Wilson, and J. C. Knowles.** 2003. The effect of increasing copper content in phosphate-based glasses on biofilms of *Streptococcus sanguis.* Biomaterials **24:**1797-1807.

30. **Mulligan, A. M., M. Wilson, and J. C. Knowles.** 2003. Effect of increasing silver content in phosphate-based glasses on biofilms of *Streptococcus sanguis.* J. Biomed. Mater. Res. A. **67A:**401-412.

31. **Oie, S., Y. Huang, A. Kamiya, H. Konishi, and T. T. Nakazawa.** 1996. Efficacy of disinfectants against biofilm cells of methicillin-resistant *Staphylococcus aureus.* Microbios. **85:**223-230.

32. **Pruitt, B. A., Jr., , A. T. McManus, S. H. Kim, and C. W. Goodwin.** 1998. Burn wound infections: current status. World. J. Surg. **22:**135-145.

33. **Saravanapavan, P., J. E. Gough, J. R. Jones, and L. L. Hench.** 2004. Antimicrobial macroporous gel-glasses: dissolution and cytotoxicity. Key. Eng. Mater. **254-256:**1087-1090.

34. **Sauer, K., A. K. Camper, G. D. Ehrlich, J. W. Costerton, and D. G. Davies.** 2002. *Pseudomonas aeruginosa* displays multiple phenotypes during development as a biofilm. J. Bacteriol. **184:**1140-1154.

35. **Schierholz, J. M., J. Beuth, and G. Pulverer.** 1999. Silver-containing polymers. J. Antimicrob. Chemother. **43:**2819-2821.

36. **Schierholz, J. M., L. J. Lucas, A. Rump, and G. Pulverer.** 1998. Efficacy of silver-coated medical devices. J. Hosp. Infect. **40:**257-262.

37. **Shiau, A. L., and C. L. Wu.** 1998. The inhibitory effect of *Staphylococcus epidermidis* slime on the phagocytosis of murine peritoneal macrophages is interferon-independent. Microbiol. Immunol. **42:**33-40.

38. **Shirtliff, M. E., J. T. Mader, and A. K. Camper.** 2002. Molecular interactions in biofilms. Chem. Biol. **9:**859-871.

39. **Sutherland, I.** 2001. Biofilm exopolysaccharides: a strong and sticky framework. Microbiology **147:**3-9.

40. **Uo, M., M. Mizuno, Y. Kuboki, A. Makishima, and F. Watari.** 1998. Properties and cytotoxicity of water soluble Na_2O-CaO-P_2O_5 glasses. Biomaterials **19:**2277-2284.

41. **Yarwood, J. M., D. J. Bartels, E. M. Volper, and E. P. Greenberg.** 2004. Quorum sensing in *Staphylococcus aureus* biofilms. J. Bacteriol. **186:**1838-1850.

662 **FIGURE LEGENDS**

663 **Figure 1.** Log_{10} CFU/mm^2 of *S.aureus* in biofilms formed on HA, Ag-, Ag10, Ag15 and
664 Ag20 discs.

665 **Figure 2.** Log_{10} CFU/mm^2 of *S. aureus* in biofilms formed on HA, Ag-, and Ag15 discs.

666 **Figure 3.** Log_{10} CFU/mm^2 of *S. aureus* in biofilms formed on HA, Ag-, and Ag20 discs.

667 **Figure 4.** CLSM images after 48h of *S. aureus* biofilms on (a) Ag- (b) Ag10 (c) Ag15
668 and (d)Ag20 discs. Viable (green) and non-viable (red) bacteria.

669 **Figure 5.** A viability profile through 2 day old biofilms grown on Ag20 discs (a). The *y*-
670 axis is the normalised viable minus nonviable fluorescence values of 3 separate viability
671 profiles. These data were further normalised to a range of 0 to1. A cross- sectional view
672 of the biofilms part used for viability profiling (b).

673 **Figure 6.** Relationship between cation and anion release rates, and rate of degradation of
674 silver-doped phosphate glasses as a function of silver content.

675 **Figure 7.** Cumulative silver ion release vs. time for Ag-, Ag10, Ag15 and Ag20 glass
676 compositions investigated.

677 **Figure 8.** ^{31}P MAS NMR spectra of the Ag-, Ag10, Ag15 and Ag20 glasses (a). A
678 highlight of the prominent peak (b)

679 **Figure 9.** HEXRD pair-distribution functions of phosphate-based glasses Ag10 (solid
680 line), Ag15 (dashed line) and Ag20 (dotted line) showing the peak due to P-O bonding.

681 **Figure 10.** Ag K-edge XANES spectra: Ag10 glass (solid line) Ag_2SO_4 (dashed line) and
682 AgO (dotted line).

683

684

685 **Table 1.** Composition of phosphate-based glasses used in this study

686

Glass code	Glass code used in the text	Glass composition (mol%)			
		Calcium Oxide	Sodium Oxide	Phosphorous Pentoxide	Silver
$Ca_{30}Na_{20}P_{50}$	Ag-	30	20	50	0
$Ca_{30}Na_{10}P_{50}Ag_{10}$	Ag10	30	10	50	10
$Ca_{30}Na_{5}P_{50}Ag_{15}$	Ag15	30	5	50	15
$Ca_{30}Na_{0}P_{50}Ag_{20}$	Ag20	30	0	50	20

Figure 1.

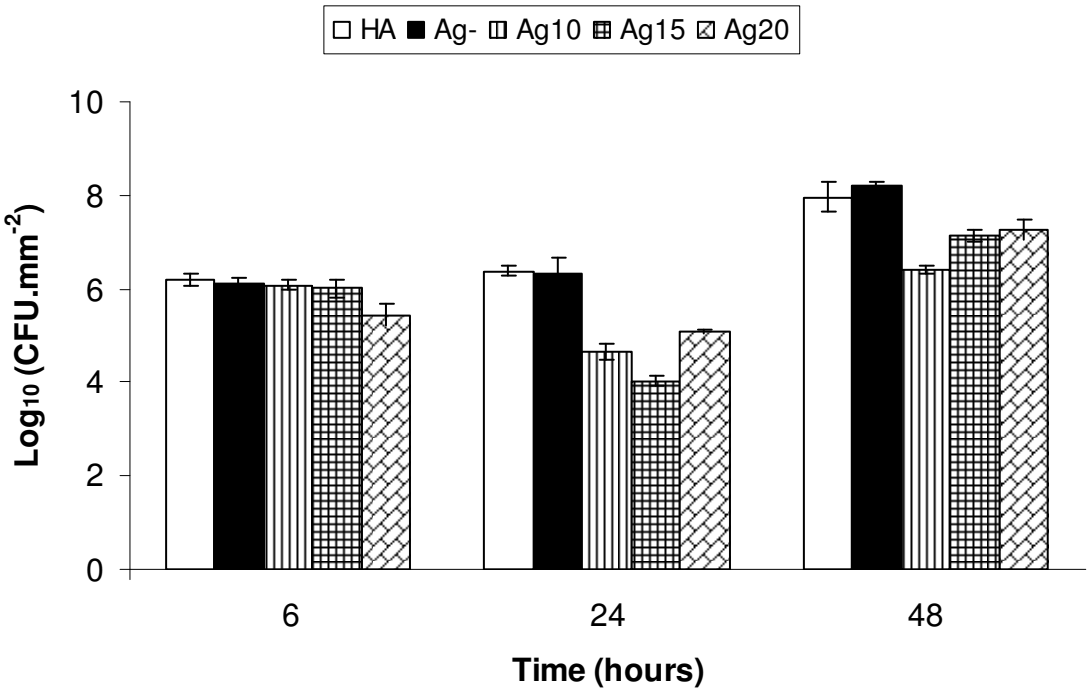

Figure 2.

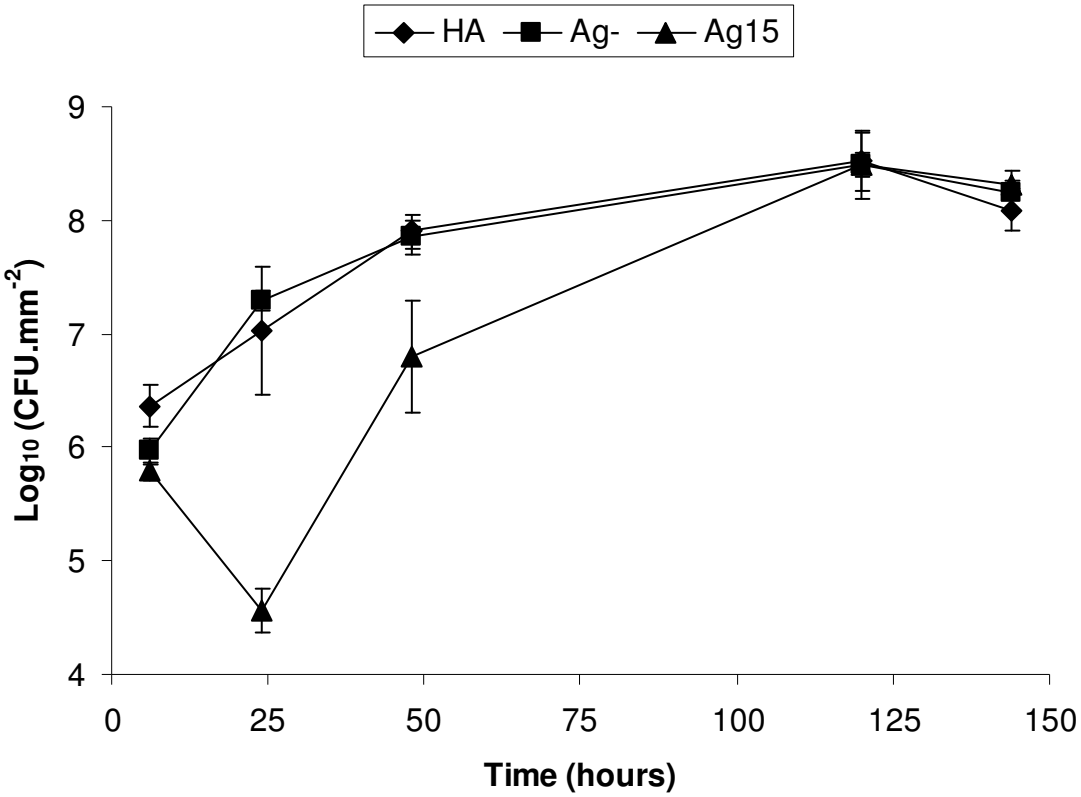
HA
Ag-
Ag15
9
8
7
6
5
4
Log10 (CFU.mm-2)
0
25
50
75
100
125
150
Time (hours)

Figure 3.

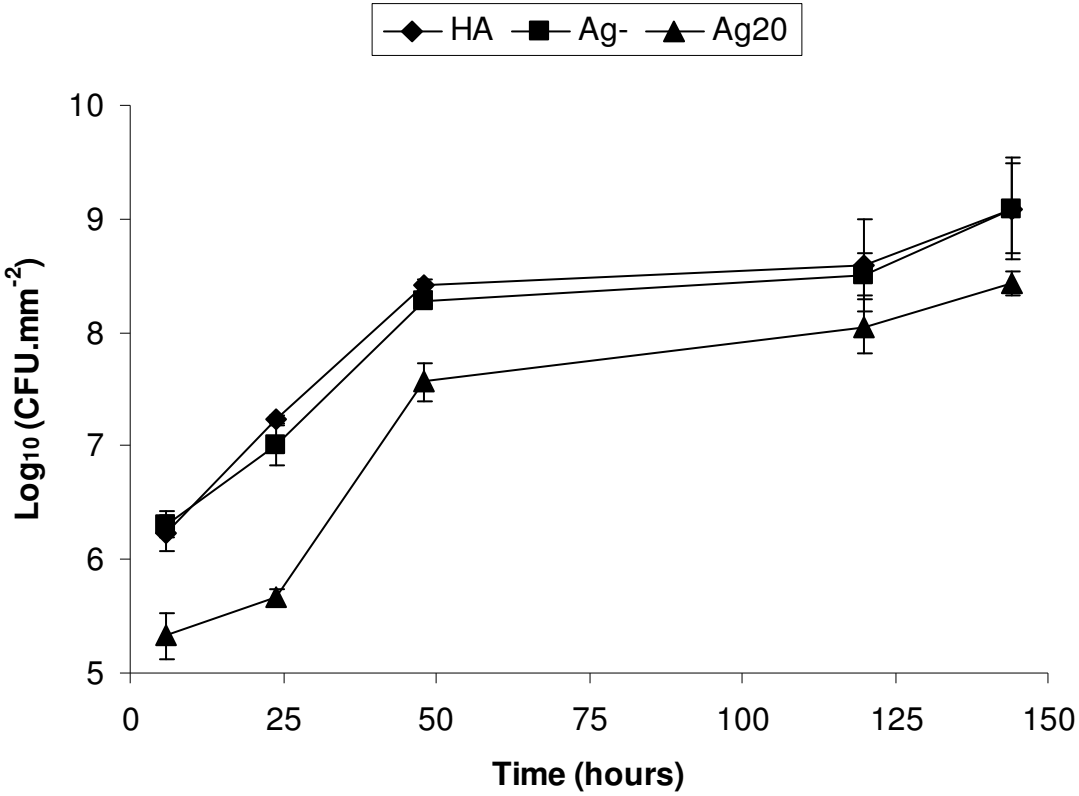
HA
Ag-
Ag20
10
9
8
7
6
5
0
25
50
75
100
125
150
Log10 (CFU.mm-2)
Time (hours)

Figure 4.

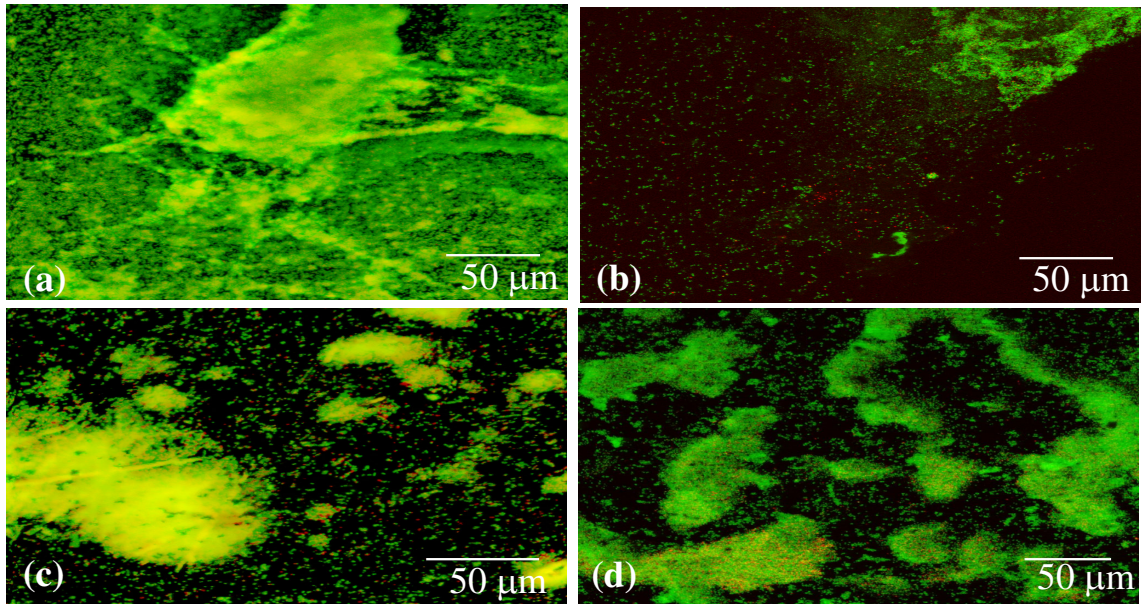

Figure 5.

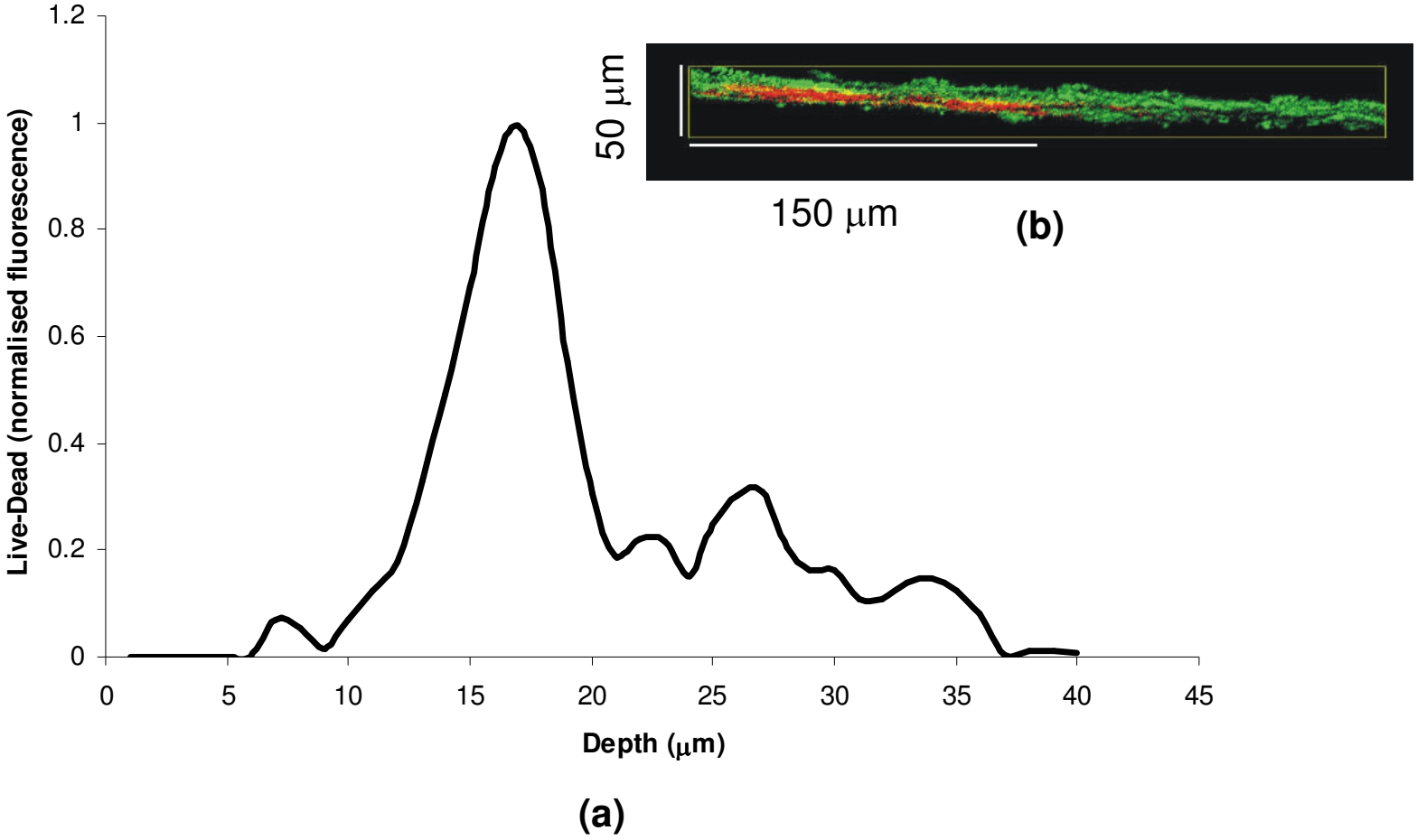
1.2
1
0.8
0.6
0.4
0.2
0
Live-Dead (normalised fluorescence)
0
5
10
15
20
25
30
35
40
45
Depth (μm)
(a)
50 μm
150 μm
(b)

Figure 6.

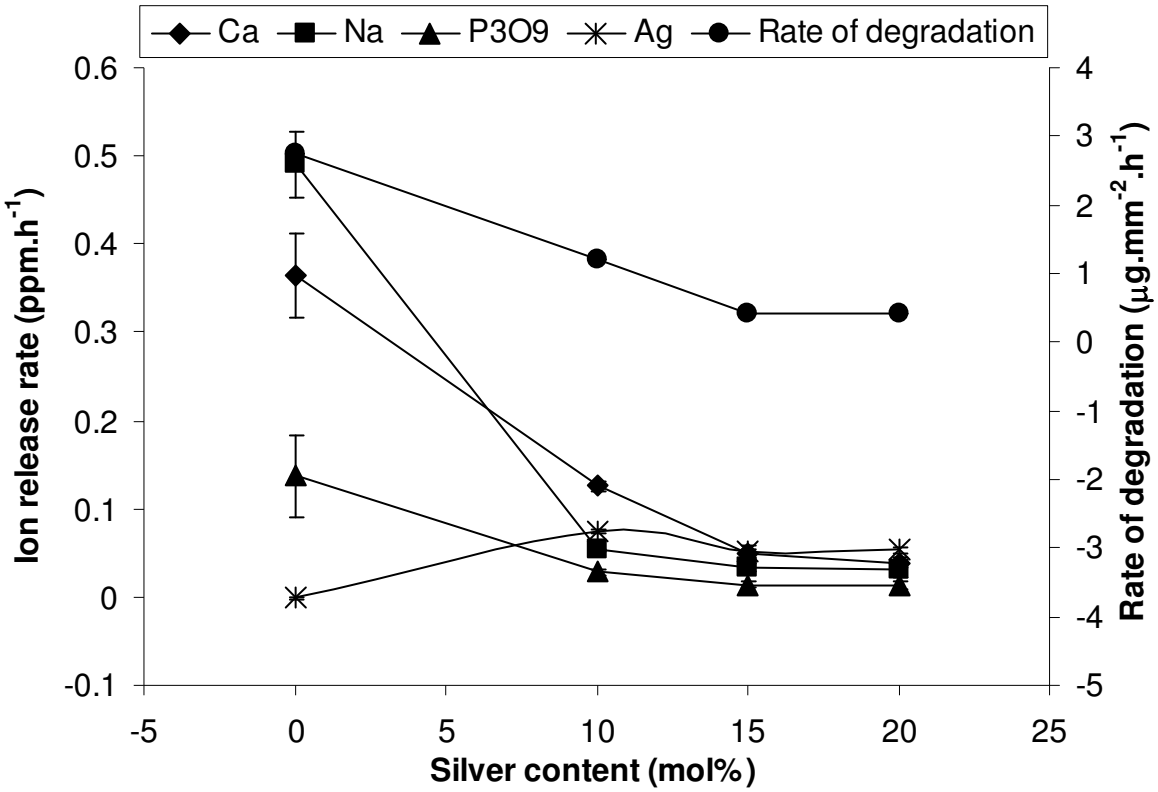
Ca
Na
P3O9
Ag
Rate of degradation
Ion release rate (ppm.h-1)
Rate of degradation (µg.mm-2.h-1)
Silver content (mol%)
0.6
0.5
0.4
0.3
0.2
0.1
0
-0.1
4
3
2
1
0
-1
-2
-3
-4
-5
-5
0
5
10
15
20
25

Figure 7.

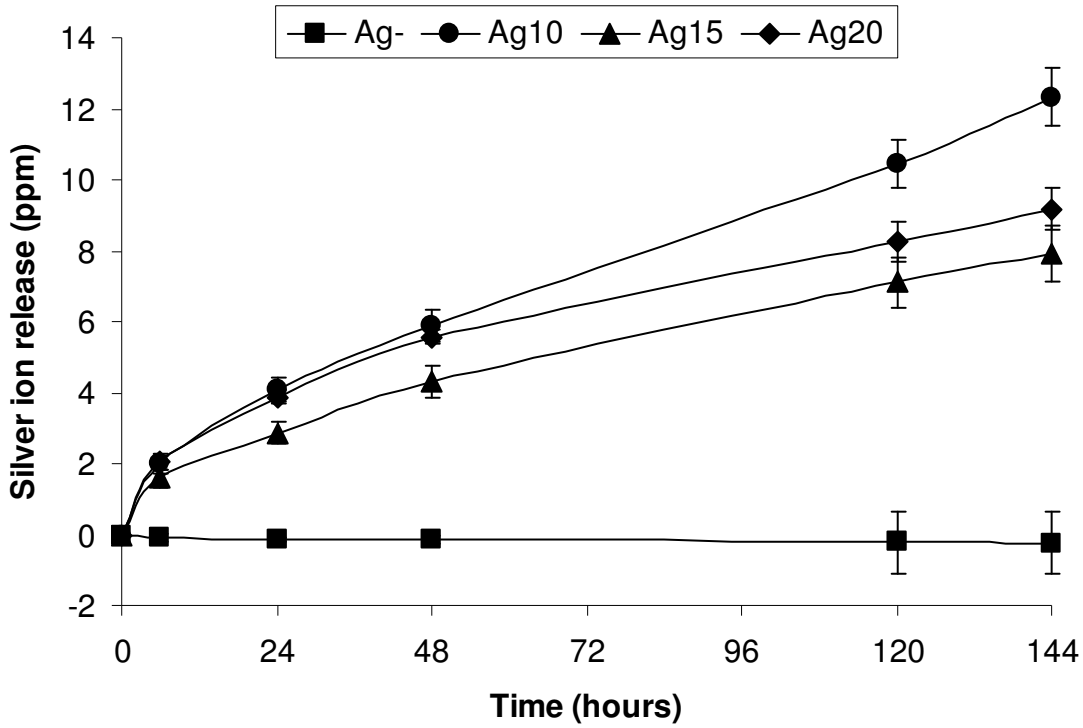
Ag-
Ag10
Ag15
Ag20
Silver ion release (ppm)
14
12
10
8
6
4
2
0
-2
0
24
48
72
96
120
144
Time (hours)

Figure 8.

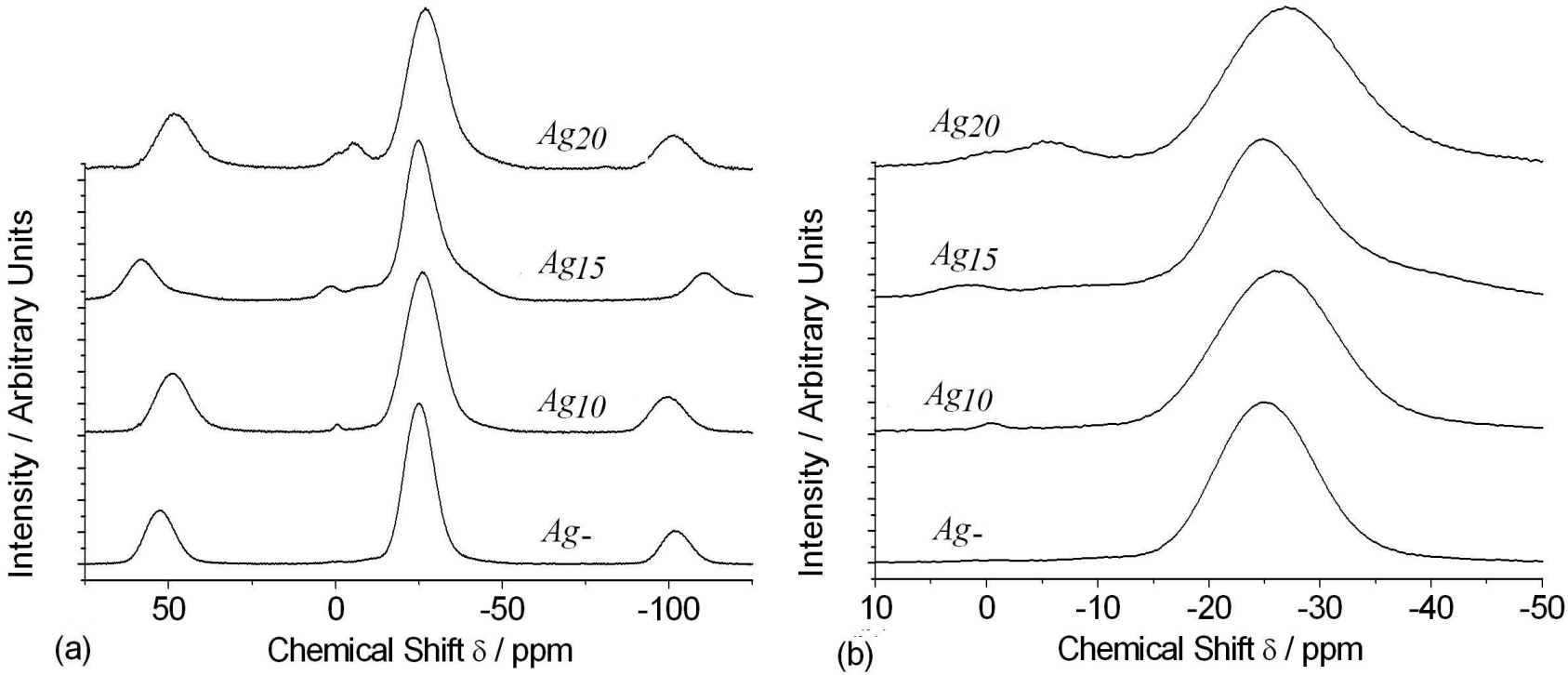
Intensity / Arbitrary Units
Ag20
Ag15
Ag10
Ag-
50
0
-50
-100
(a)
Chemical Shift δ / ppm
Intensity / Arbitrary Units
Ag20
Ag15
Ag10
Ag-
10
0
-10
-20
-30
-40
-50
(b)
Chemical Shift δ / ppm

Figure 9.

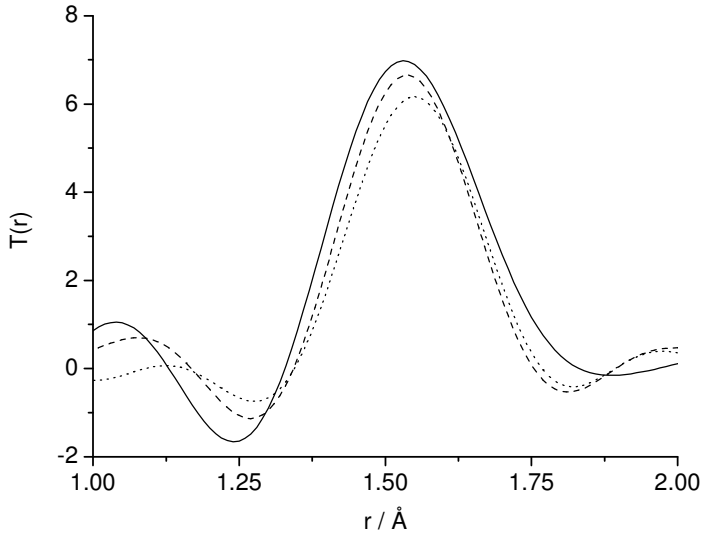

Figure 10.

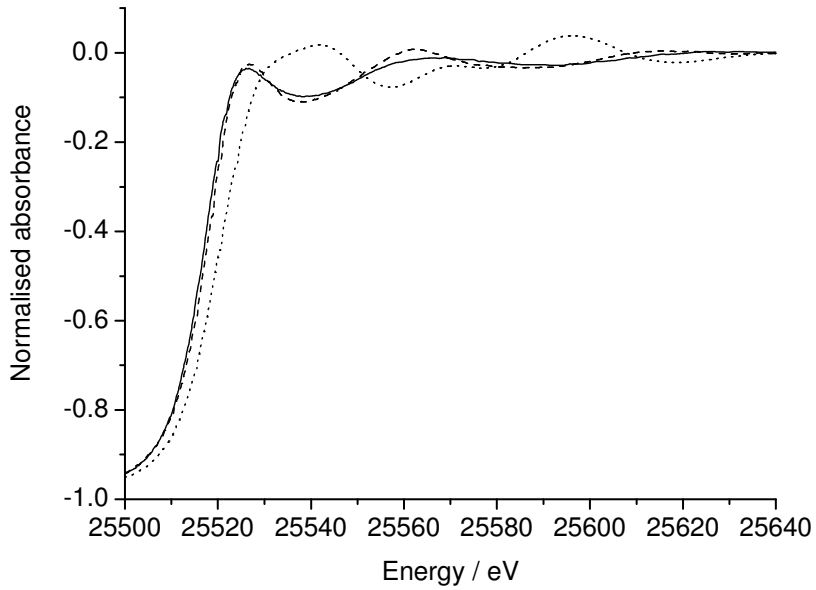
Normalised absorbance
0.0
-0.2
-0.4
-0.6
-0.8
-1.0
25500
25520
25540
25560
25580
25600
25620
25640
Energy / eV